Design of High-Speed MUTC-PD With Electric Field Regulation Layer

Jian-bo Xu, Kai Liu*, Xiao-wen Dong, Xiao-feng Duan, Yong-qing Huang, Qi Wang and Xiao-min Ren

State Key Laboratory of Information Photonics and Optical Communications, Beijing University of Posts and Telecommunications, Beijing 100876, China

School of Electrical Engineering, Beijing University of Posts and Telecommunications, Beijing 100876, China

Abstract: A novel modified uni-traveling-carrier photodiode (MUTC-PD) with an electric field regulation layer, which is a p-type doped thin layer inserted behind the PD's n-doped cliff layer, is proposed. The added electric field regulation layer can not only decrease and smooth the electric field intensity in the PD's collector layer and make photo-generated electrons transit there at its peak drift velocity, but also can improve the electric field intensity in the PD's depleted absorber layer and optimize the photo-generated carriers' saturated transit performance in it. Moreover，it will also be beneficial for the PD's parasitic capacitance effect, since a long collector layer can be designed to reduce the PD's junction capacitance, and the electron's peak drift velocity can compensate for the lost transit time. Thus, the 3-dB bandwidth of the PD's photo-response will be optimized. The final performance optimization obtains a MUTC-PD with a 3-dB bandwidth of 68 GHz at a responsivity of 0.502 A/W. And it can be used for 100 Gbit/s optical receivers.

Key words: peak electron drift velocity; transit performance; MUTC-PD; optical fiber communication; optical interconnect

具有电场调控层的高速 MUTC-PD 设计

徐建波，刘凯*,董晓雯，段晓峰，黄永清,王琦，任晓敏

（信息光子学与光通信全国重点实验室，北京邮电大学，北京 100876）

(电子工程学院，北京邮电大学，北京 100876)

摘要: 本文提出了一种具有电场调控层的新型改进型单行载流子光探测器（MUTC-PD）。该光探测器中，崖层后新增的 p 型掺杂电场调控层能够优化收集层中的电场强度，使光生电子在收集层中以峰值漂移速度输运；同时能够增强耗尽吸收层中的电场强度，优化其中光生载流子饱和速度输运特性；并且，器件收集层中光生电子的峰值漂移速度输运特性可以进一步优化其寄生电容特性，从而显著提升光探测器的 3dB 响应带宽。经过仿真优化设计，获得了响应度为 0.502 A/W，3-dB 带宽为 68 GHz 的 MUTC-PD，可应用于 100 Gbit/s 光接收机。

关键词: 电子峰值速度；输运特性；改进型单行载流子光探测器；光纤通信；光互连

中图分类号: TN215

1. Introduction

To meet the exponential growth demand for data traffic capacity in data centers, photodetectors are required to quickly respond to 100 Gbps signals with high sensitivity. Nowadays, port transmission rate of 400 Gb/s is being scaled up in data centers. Transceiver modules with 800 Gb/s port rate are now undergoing small-scale trials, and those with 1.6 Tb/s port rate have entered the prototype stage. Corresponding port rate standards include 8×200 Gb/s, 8×100 Gb/s, etc., with different modulation schemes. This necessitates the development of high-speed photodetectors capable of supporting these standards, with their photo-response bandwidth exceeding 57 GHz and responsivity over 0.5 A/W, for applications in single-wavelength 100 Gb/s optical channels [1]. To accomplish the PD performance required, many attempts had been conducted, such as mushroom-type photodetectors [2], dual-absorption-layer photodetectors [3], PIN photodetectors [4], PDA-PDs [5], and uni-traveling-carrier photodiode (UTC-PD) [6], etc. Among them, the UTC-PD, which was firstly proposed in 1997, effectively mitigates the space-charge effect in PIN PD by using electron as single transit carrier to promote its high speed performance [6]. And then, MUTC-PD optimizes the UTC-PD's absorber layer by dividing it into a p-doped region and a depleted region to obtain high speed and high responsivity performance simultaneously [7][8]. However, in pursuit of enhanced high-speed performance, MUTC-PD typically features thin absorber layers, resulting in lower responsivity. By increasing the thickness of the absorber layer, a greater responsivity can be obtained, but it increases the transit time of carrier and decreases the bandwidth of the PD. To reduce the degradation of the PD's response bandwidth caused by the thick absorption layer, one applicable method is to increase the mean electron transit velocity [9-11].

In this paper, a novel MUTC-PD structure with an electric field regulation layer inserted between its cliff layer and its collector layer is proposed for performance optimization. By optimizing the doping concentration of the electric field regulation layer and the thickness of the collector layer, the electric field intensity inside the MUTC-PD's collector layer can be tuned at certain level to make the photo-generated electrons transit in it at their peak drift velocities constantly. At the same time, the electric field intensity in the PD's absorber could be optimized to make sure that, in its depleted region the photo-generated hole would transit at its saturated drift velocity and in its p-doped region the photo-generated electron's diffusion enhancement factor could be maximized. Moreover, as in the proposed novel MUTC-PD, the electron transit at its peak drift velocity in the PD's collector layer, the PD's parasitic capacitance can be further optimized. Such performance and their overall impact on the PD's high speed photo-response are analyzed. In the analysis, for better

coupling of the incident light, the diameter of the PD is set to be 16 μm. In the following context, the proposed MUTC-PD will be referred to as the swift-responding modified uni-traveling-carrier photodiode (SMUTC-PD) to distinguish it from the MUTC-PD.

2. SMUTC-PD DESIGN

The epitaxial structure of the SMUTC-PD is shown in Fig. 1. Above the SI-InP substrate, a 500 nm thick InP buffer layer with an n-doping level of 5×10^{18} cm^{-3} is deposited. On top of it, an un-intentionally doped InP collector layer is placed, which thickness is set to be x nm for further optimization. Above the collector layer, a 20 nm thick InP electric field regulation layer with a p-doping level of 1×10^{16} cm^{-3} is designed, which can regulate the electric field intensity distribution in the collector layer. The next, a 80 nm thick InP cliff layer with a n-doping level of 7.2×10^{16} cm^{-3}, a 40 nm thick InGaAsP layer (Q1.24) with a p-doping level of 5×10^{15} cm^{-3} and a 40 nm thick InGaAsP layer (Q1.46) with a p-doping level of 5×10^{15} cm^{-3} were placed one by one consecutively. Q1.24 and Q1.46 represent the cut-off wavelengths of the corresponding InGaAsP materials. Then, a 100 nm thick un-intentionally doped InGaAs layer and a 350 nm thick p-doped InGaAs layer with a doping level of 3.5×10^{16} cm^{-3} were grown as absorption region of the PD. Above it, a 50 nm thick InGaAsP electron block layer with a p-doping level of 1×10^{19} cm^{-3} is grown. The top most cap layer is a 50 nm thick p-doped InGaAs layer with a doping level of 1×10^{19} cm^{-3}.

p-InGaAs $1x10^{19}cm^{-3}$ 50nm
p-InGaAsP $1x10^{19}$ cm^{-3} 50 nm (Q1.12)
p-InGaAs $3.5x10^{16}$ cm^{-3} 350 nm
p-InGaAs $1x10^{15}cm^{-3}$ 100 nm
p-InGaAsP $5x10^{15}$ cm^{-3} 40 nm (Q1.46)
p-InGaAsP $5x10^{15}$ cm^{-3} 40 nm (Q1.24)
n-InP $7.2x10^{16}$ cm^{-3} 80 nm
p-InP $1x10^{16}$ cm^{-3} 20 nm
n-InP $1x10^{15}$ cm^{-3} x nm
n-InP $5x10^{18}$ cm^{-3} 500 nm
n-InP Substrate 500 nm

Fig. 1 Epitaxial Layer Scheme

In the context, SMUTC-PD's performance simulations are conducted with Silvaco Atlas. For analyzing its parasitic performance, an extra 15 Ω series resistance is added to the ideal 50 Ω load resistance. And also, an extra parallel parasitic capacitance of 5 fF is added to simulate the capacitance introduced by the metal contact pad. To analyze the electron's peak drift velocity performance in InP, the

negative differential mobility model is used. The bias voltage in the simulation is set to 3V. The material parameters of InP, InGaAsP and InGaAs are obtained from Ref. [12-15]. And the optical and electrical parameters of the materials used in the simulation (InP and InGaAs) are given in Table 1.

Table 1 - Material parameters used in the simulation

Parameter	InP	InGaAs
Electron mobility, μ_n	5400 cm^2/Vs	12000 cm^2/Vs
Hole mobility, μ_p	200 cm^2/Vs	300 cm^2/Vs
Conduction band density of states, Nc	1.1×10^{19} cm^{-3}	7.7×10^{18} cm^{-3}
Valence band density of states, Nv	5.7×10^{17} cm^{-3}	2.1×10^{17} cm^{-3}
Electron Staturation velocity	2.6×10^{7} cm/s	2.5×10^{7} cm/s
Hole staturation velocity	5×10^{6} cm/s	5×10^{6} cm/s
Electron and Hole lifetime	2×10^{-9} s	1×10^{-7} s
Electron Auger coefficient	3.7×10^{-31} cm^6/s	3.2×10^{-28} cm^6/s
Hole Auger coefficient	8.7×10^{-30} cm^6/s	3.2×10^{-28} cm^6/s
Real refractive index	3.2	3.51
Imaginary refractive index	0	0.106

As stated above, the SMUTC-PD introduces an electric field regulation layer (EFRL) to optimize the photo-generated electrons' and holes' transit performance. The transit bandwidth of SMUTC-PD is determined by the electron's transit time in the collector layer, the p-doped absorption layer, and by the hole's transit time in the depleted absorption layer. The doping level of the EFRL is used to optimize the above parameters by adjusting the electric field intensity distribution in the above mentioned three layers. And the simulation results are shown in Fig. 2. Electron and hole's transit velocity distributions in the SMUTC-PD with different doping-level in EFRL are shown in Fig. 3 and Fig. 4. In the above analysis, the thickness of collector layer is set to be 900 nm. Fig. 2 shows that, the introduction of the EFRL makes the electric field intensity distribution in the collector layer consistent, and thus the electrons can transit at a uniform velocity throughout the collector layer. Moreover, the optimization of the electric field intensity distribution in the collector layer and the depleted absorption region can be achieved by adjusting the doping of the EFRL, which is set to D_0. When reducing the value of D_0, the electric intensity in collector layer can be lowered down (as shown in Fig. 2) and make it approaching to the level that make the electrons transit in it with the peak electron drift velocity, as shown in Fig. 3. At the same time, the electric intensity in depleted absorption layer will be increased (as shown in Fig. 2) and make the holes' transit velocity approaching their maximum level (the saturated hole drift velocity), as shown in Fig. 4.

As shown in Fig. 2, the electric field intensity in collector layer rises from 13 kV/cm to 30 kV/cm when D_0 goes from 3×10^{16} cm^{-3} to 5×10^{17} cm^{-3}. Specially, the electric field intensity in collector layer is approximated to be 11 kV/cm when D_0 is 1×10^{15} cm^{-3} and 1×10^{16} cm^{-3}. In this range, the electrons can transit in InP at its peak drift velocity of 4×10^{7} cm/s. And this is verified by the simulation analysis of the electron's transit velocity distribution in the SMUTC-PD, which is shown in Fig. 3. Furthermore, when D_0 goes from 3×10^{16} cm^{-3} to 5×10^{17} cm^{-3}, the mean velocity of electrons in collector layer decreases from 3.8×10^{7} cm/s to 2.8×10^{7} cm/s.

Also shown in Fig. 2, when D_0 is 1×10^{15} cm^{-3} and 1×10^{16} cm^{-3}, in depleted absorption region, the electric field intensity is approximated to be 86 kV/cm, and the velocity of holes is 4.3×10^{6} cm/s as shown in Fig. 4, approaching its saturated drift velocity. From Fig. 2 and 4, one can see that the electric field intensity decreases from 85 kV/cm to 47 kV/cm when D_0 goes from 3×10^{16} cm^{-3} to 5×10^{17} cm^{-3}, and the maximum velocity of holes decreases from 4.2×10^{6} cm/s to 3.7×10^{6} cm/s. Simultaneously, the electrons consistently transit at their saturation drift velocity of 2.5×10^{7} cm/s.

And in p-doped absorption region, the hole relaxes. When D_0 is 1×10^{15} cm^{-3} and 1×10^{16} cm^{-3}, the minimum velocity of electrons is 1.0×10^{7} cm/s and 9.3×10^{6} cm/s according to Fig. 3. When D_0 goes from 3×10^{16} cm^{-3} to 5×10^{17} cm^{-3}, the minimum velocity of electrons decreases from 7.9×10^{6} cm/s to 2.2×10^{6} cm/s.

In summary, in the above three layers, when D_0 is 1×10^{15} cm^{-3} and 1×10^{16} cm^{-3}, the transit performance of electrons and holes can be optimized. Ultimately, the doping concentration of 1×10^{16} cm^{-3} is chosen for the EFRL layer, as in the above three layers, the collector layer is longer and has a greater impact on the PD's high-speed characteristics.

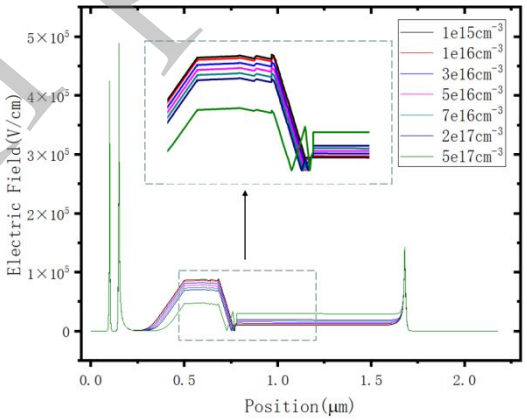

Fig. 2 Electric field intensity distribution in SMUTC-PD at different doping concentrations in the electric field regulation layer

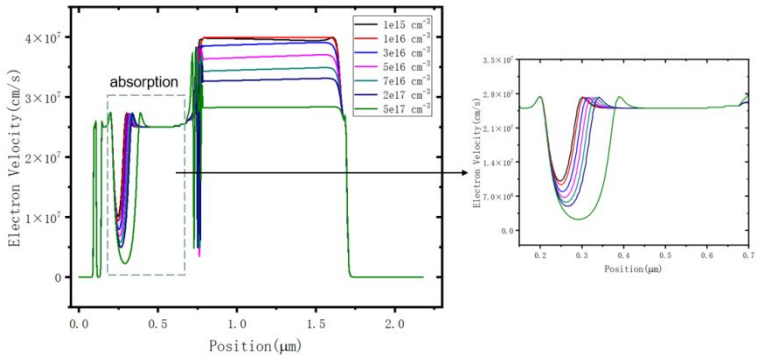

Fig. 3 Electron velocity distributions of SMUTC-PD at different doping concentrations in the electric field regulation layer

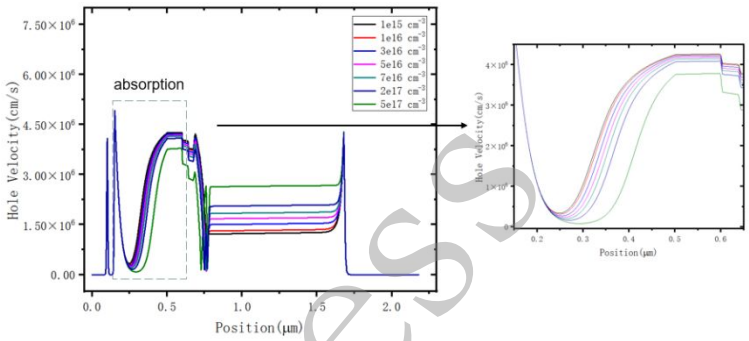

Fig. 4 Hole velocity distributions of SMUTC-PD at different doping concentrations in the electric field regulation layer

3. SMUTC-PD PERFORMANCE ANALYSIS

When optimizing the SMUTC-PD's dynamic photo-response performance, its collector layer's thickness is a major influencing factor. It determines the majority of the photo-generated electrons' transit time and also the PD's junction capacitance. So that, the thickness of the PD's collector layer and the electric field intensity distribution in it need to be carefully designed. To improve the PD's dynamic performance, its collector's thickness can be increased to reduce its parasitic capacitance. At the same time, by optimizing the electric field intensity distribution in the PD's collector as stated in section Ⅱ, the photo-generated electrons can transit through the PD's collector with its peak drift velocity. And then the increment of electron's transit time in collector can be compensated.

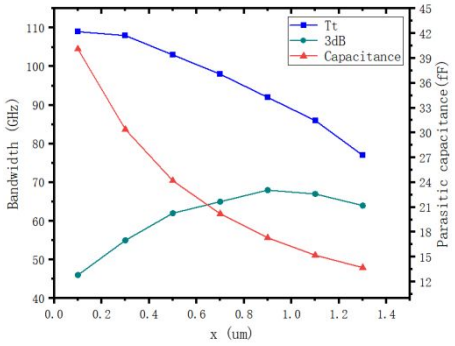

Fig. 5 SMUTC-PD's Frequency response and parasitic capacitance with different collector layer thicknesses

In the SMUTC-PD optimization, the PD collector's thickness x is changing from 0.1 μm to 1.3 μm. And the PD's photo-response bandwidth is calculated correspondingly. The simulated PD's carrier transit time determined photo-response bandwidth is denoted as "Tt" and blue solid line with square mark in Fig. 5-7. At the same time, the parasitic capacitance simulated from SMUTC-PD structure is shown in Fig. 5-7 as "capacitance" and red solid line with triangle mark. The total PD's photo-response bandwidth resulted from carriers' transit time and PD's parasitic effect in the simulation is denoted as "3dB" and green solid line with circle mark in Fig. 5-7. As shown in Fig. 5, at the 3V reverse bias voltage, in the collector's thickness x changing range, the transit time determined bandwidth of the PD decreases continuously from 109 GHz to 77 GHz, but the total bandwidth rises to a peak of 68 GHz at x=0.9 μm, and then decreases. Therefore, the collector layer thickness is optimized to be 900 nm. As stated in section 2, the doping concentration of the EFRL will affect the electric field intensity distribution in the collector layer, and then determine the mean electron transit velocity in it. In the simulations shown in Fig. 5, the mean electron transit velocity is optimized to its peak drift velocity.

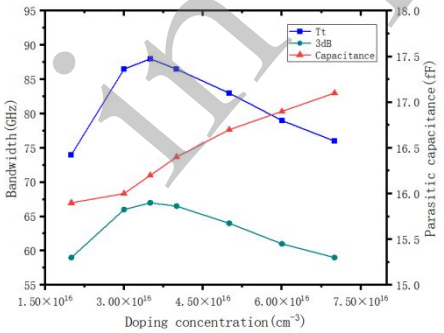

Fig. 6 SMUTC-PD's photo-response bandwidth and parasitic capacitance with different doping concentrations in the p-doped absorption

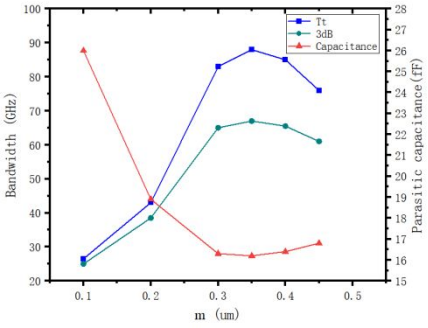

Fig. 7 SMUTC-PD's photo-response bandwidth and parasitic capacitance with different thicknesses of the p-doped absorption region

In order to investigate the effect of the doping concentration and thickness of the p-doped absorption region on the SMUTC-PD's photo-response bandwidth, its

doping concentration is set changing from 3×10^{16} cm^{-3} to 7×10^{16} cm^{-3} for short enough hole relaxation time, and its thickness is denoted as m μm. Then the thickness of the depleted absorption region is set to (0.45-m) μm. The SMUTC-PD's frequency photo-response performance is simulated to determine the optimal doping concentration in p-doped absorption region [16]. Fig. 6 shows the simulation results for different p-doped absorption region's doping levels, and Fig. 7 shows that for different m values. And the optimal doping level for p-doped absorption region is determined to be 3.5×10^{16} cm^{-3}, while the optimal thickness for it is determined to be 0.35 μm.

Next, the effect of electron transit characteristic in SMUTC-PD's collector layer on the PD's parasitic capacitance would be analyzed. According to Ref. [17][18], this electron's transit velocity determinzed capacitance can be expressed by the following equation:

$$c = -\frac{dQ}{dv} = -i\frac{d\tau}{dV} = rP\frac{dv}{v^2 dE} \tag{1}$$

where dQ is the change in electric charge for a given change in voltage, dV. It can be concluded that this capacitance depends on the differentiation of the electron transit velocity with respect to the electric field intensity determining it, i.e., the curve slope of the electron transit velocity versus electric field intensity. And it can further reduce the SMUTC-PD's parasitic capacitance while the electron transit around its peak drift velocity. Finally, Fig. 8 depicts the frequency response of the optimized SMUTC-PD and that of a MUTC-PD with the same structure except for the EFRL. The results show that the SMUTC-PD obtains a 3-dB bandwidth of 68 GHz, which is far greater than the MUTC-PD's 54 GHz 3-dB bandwidth, while the incident optical power is set to 1 mW only. According to Ref. [17], for a standard MUTC-PD, it needs large incident optical power to regulate the electric field intensity in PD's collector layer to obtain electron's peak drift velocity in it. Thus, the proposed SMUTC-PD overcomes such limitations.

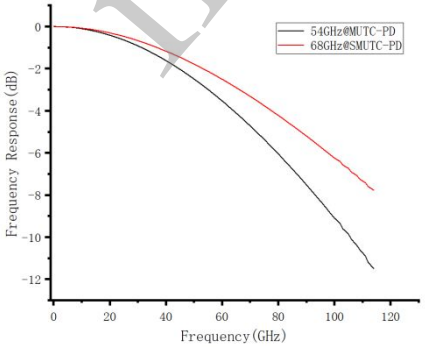

Fig. 8 SMUTC-PD's Frequency response

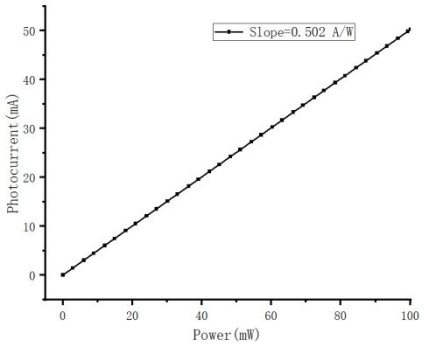

Fig. 9 SMUTC-PD's responsivity

According to [19], the reflectivity of the top electrode is set to be 0.6. As shown in Fig. 9, the responsivity of SMUTC-PD is 0.502 A/W, while absorption layer thickness is set to be 0.45 μm.

4. Conclusion

In conclusion, this paper proposes a novel SMUTC-PD for 100 Gbit/s optical receivers. The electric field intensity in the collector layer is optimized by introducing an electric field regulation layer after the cliff layer, ensuring that electrons consistently operate at peak velocity to offset the increased electron transit time caused by the extended collector layer, while also achieving reduced capacitance. Additionally, this layer can redistribute the voltage between the absorption and collector layers, further enhancing the device's overall performance. Moreover, the device exhibits robust performance under low-power conditions, independent of incident optical power fluctuations. Ultimately, an optimal 3-dB bandwidth of 68 GHz with a responsivity of 0.502 A/W is attained, marking a significant 25.9% bandwidth enhancement compared to the original MUTC-PD's 54 GHz bandwidth. These findings demonstrate that the SMUTC-PD, featuring an electric field regulation layer, can effectively enhance the photodetector's high-speed performance, offering a promising solution for improving device bandwidth.

Acknowledgements

This research was supported in part by the National Natural Science Foundation of China (grant No. 62374020), in part by the Zibo Science and Technology SMEs Innovation Capacity Improvement Project (grant No. 2022tsgc0046), and in part by the Shandong Science and Technology SMEs Innovation Capacity Improvement Project (grant No. 2022TSGC2290).

References:

[1] PAOLUCCI F, SGAMBELLURI A, EMMERICH R, et al. Openconfig control of 100G/400G filterless metro networks with configurable modulation format and FEC [J]. *Optical Fiber Communication Conference*, 2019. doi: 10.1364/OFC.2019.Tu3H.4

[2] ZHANG K R, HUANG Y Q, DUAN X F. Design and analysis of hybrid integrated high-speed mushroom vertical PIN photodetector [J]. *Applied Mechanics and Materials*, 2013,411-414:1455-1458. doi: 10.4028/www.scientific.net/AMM.411-414.1455

[3] EFFENBERGER F J, JOSHI A M. Dual-depletion double-pass InGaAs photodetectors for efficient high-speed operation [J]. *Journal of Lightwave Technology,* 1996,14(8): 1859-1864.

[4] KATO K, HATA S, KAWANO K, et al. Design of ultrawide-band, high sensitivity pin photodetectors [J]. *IEICE transactions on electronics*, 1993, 76(2): 214-221.

[5] LI X, DEMIGUEL S, LI N, et al. Backside illuminated high saturation current partially depleted absorber photodetectors [J]. *Electronics Letters*, 2003, 39(20): 1466-1467. doi: 10.1049/el:20030927

[6] ISHIBASHI T, ITO H. Uni-traveling-carrier photodiodes [J]. *Journal of Applied Physics*, 2020, 127(3). doi: 10.1063/1.5128444

[7] LI Q, LI K, FU Y, et al. High-power flip-chip bonded photodiode with 110 GHz bandwidth [J]. *Journal of Lightwave Technology*, 2016, 34(9): 2139-2144. doi: 10.1109/jlt.2016.2520826

[8] SRIVASTAVA S. Simulation study of InP-based uni-traveling carrier photodiode [D]. University of Cincinnati, 2003.

[9] JIN L, BING X, LUO Y, et al. Ultrafast dual-drifting layer uni-traveling carrier photodiode with high saturation current [J]. *Optics Express*, 2016, 24(8): 8420-8428. doi: 10.1364/OE.24.008420

[10] CHAO E, XIONG B, SUN C, et al. D-band MUTC photodiodes with flat frequency response [J]. *IEEE Journal of Selected Topics in Quantum Electronics*, 2021, 28(2) : 1-8. doi: 10.1109/JSTQE.2021.3115488

[11] ZHEN Z, HAO R, XING D, et al. Near-ballistic optimization design of high-speed single-line charge carrier photodiodes [J]. *Chinese Journal of Lasers*, 2020, 47(10): 195-202.

[12] ADACHI S. Physical properties of III-V semiconductor compounds [M]. John Wiley & Sons, 1992.

[13] SHRESTHA Y R. Numerical simulation of GaAsSb/InP uni-traveling carrier photodiode [D], University of Cincinnati, 2005.

[14] ISHIBASHI T, FURUTA T, FUSHIMI H, et al. InP/InGaAs uni-traveling-carrier photodiodes [J]. *IEICE transactions on electronics*, 2000, 83(6): 938-949.

[15] FRIESE, S. Atlas. ti 8 Mac-user manual updated for program version 8.4. ATLAS. ti, Berlin, 2019.

[16] ZHANG P, ZHANG X, ZHANG R. Design of broadband and high-output power uni-traveling-carrier photodiodes [J]. *Optics Communications*, 2016, 365: 194-207. doi: 10.1016/j.optcom.2015.11.075

[17] ZHOU G, RUNGE P. Nonlinearities of high-speed pin photodiodes and MUTC photodiodes [J]. *IEEE Transactions on Microwave Theory and Techniques*, 2017, 65(6): 2063-2072. doi: 10.1109/TMTT.2016.2645152.

[18] DONG X, LIU K, HUANG Y, et al. Design of high-speed UTC-PD with optimization of its electron transit performance and parasitic capacitance [J]. *IEEE Photonics Journal*, 2023, 15(1): 1-9. doi: 10.1109/JPHOT.2023.3234063

[19] SAKAI K, ISHIMURA E, NAKAJI M, et al. High-current back-illuminated partially depleted-absorber p-i-n photodiode with depleted nonabsorbing region [J]. *IEEE*

Transactions on Microwave Theory and Techniques, 2010, 58(11): 3154-3160. doi: 10.1109/TMTT.2010.2075470

Author Biography：

KAI LIU received the bachelor's degree in applied electronic technology and the Ph.D. degree in fiber optic communications and optoelectronics from the Beijing University of Posts and Telecommunications (BUPT), China, in 1994 and 1999, respectively. He made a Postdoctoral Project on the research of optical pumped 1.3μm VCSEL at the University of Southern California, Los Angeles, CA, USA, in 2000 and 2001.

He is currently an Associate Professor with the School of Electrical Engineering, BUPT. He is the author of more than 20 refereed journal articles and conference papers in the field of optoelectronic technology. His current research interests include optical interconnects, optoelectronics integration, and photonic device for optical fiber communications. Recently, he has made contributions to the single mode VCSEL for optical interconnects and high speed, high power UTC-PD for radio on fiber system.